

# RSC Advances



This is an *Accepted Manuscript*, which has been through the Royal Society of Chemistry peer review process and has been accepted for publication.

*Accepted Manuscripts* are published online shortly after acceptance, before technical editing, formatting and proof reading. Using this free service, authors can make their results available to the community, in citable form, before we publish the edited article. This *Accepted Manuscript* will be replaced by the edited, formatted and paginated article as soon as this is available.

You can find more information about *Accepted Manuscripts* in the [Information for Authors](#).

Please note that technical editing may introduce minor changes to the text and/or graphics, which may alter content. The journal's standard [Terms & Conditions](#) and the [Ethical guidelines](#) still apply. In no event shall the Royal Society of Chemistry be held responsible for any errors or omissions in this *Accepted Manuscript* or any consequences arising from the use of any information it contains.

## Direct electrochemistry of cytochrome *c* immobilized on a graphene oxide-carbon nanotube composite for picomolar detection of hydrogen peroxide

Bose Dinesh<sup>a</sup>, Veerappan Mani<sup>b</sup>, Ramiah Saraswathi<sup>a\*</sup>, Shen-Ming Chen<sup>b</sup>

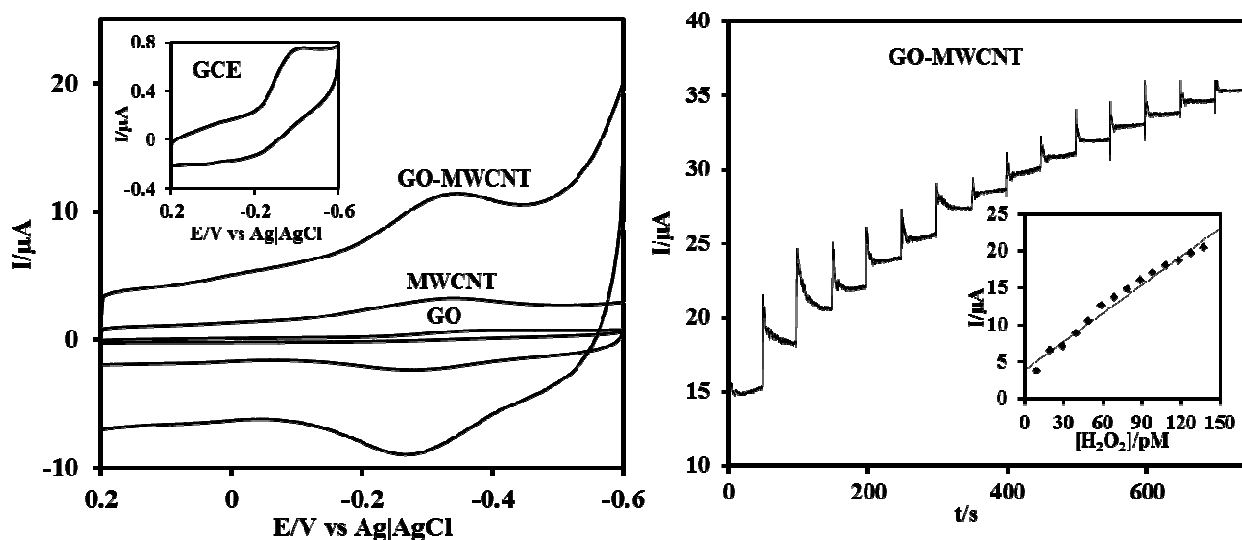
<sup>a</sup>Department of Materials Science, School of Chemistry, Madurai Kamaraj University, Madurai – 625 021, Tamilnadu, India

<sup>b</sup>Department of Chemical Engineering and Biotechnology, National Taipei University of Technology, No.1, Section 3, Chung-Hsiao East Road, Taipei 106, Taiwan, ROC.

E-mail: [saraswathir@yahoo.com](mailto:saraswathir@yahoo.com)

### Graphical Abstract

A highly efficient direct electron transfer in a new bioelectrode *viz.* cytochrome *c* immobilized graphene oxide-multiwalled carbon nanotube on a nano gold modified glassy carbon electrode is demonstrated. The biocompatible graphene oxide greatly enhances the immobilization of cytochrome *c* while the highly conducting multi-walled carbon nanotube helps to achieve a faster kinetics of the electron transfer. The bionanocomposite modified electrode is used to fabricate a highly selective and sensitive amperometric biosensor for the picomolar level detection of hydrogen peroxide which may find application in bioimaging and healthcare.



**Direct electrochemistry of cytochrome *c* immobilized on a graphene oxide-carbon nanotube composite for picomolar detection of hydrogen peroxide**

Bose Dinesh<sup>a</sup>, Veerappan Mani<sup>b</sup>, Ramiah Saraswathi<sup>a\*</sup>, Shen-Ming Chen<sup>b</sup>

<sup>a</sup>Department of Materials Science, School of Chemistry, Madurai Kamaraj University,  
Madurai – 625 021, Tamilnadu, India

<sup>b</sup>Department of Chemical Engineering and Biotechnology, National Taipei University of  
Technology, No.1, Section 3, Chung-Hsiao East Road, Taipei 106, Taiwan, ROC.

Corresponding author. Tel.: +91 452 2458247; Fax: +91 452 2459181.

e-mail address: drsaraswathi@gmail.com (R. Saraswathi).

## Abstract

We describe the fabrication of an amperometric biosensor based on cytochrome *c* (Cyt *c*) immobilized graphene oxide - multiwalled carbon nanotube (GO-MWCNT) composite on a nano Au modified glassy carbon electrode for trace level detection of H<sub>2</sub>O<sub>2</sub>. Morphology and surface characterization of the nanocomposite reveal the successful formation of a highly conducting MWCNT network on the GO surface. Electrochemical impedance studies indicate a lower charge transfer resistance compared to the bare electrode. Cyclic voltammetry studies clearly demonstrate an enhanced direct electrochemistry of Cyt *c* with a high electron transfer rate constant ( $k_s$ ) value of 3.4 s<sup>-1</sup>. An amperometric H<sub>2</sub>O<sub>2</sub> biosensor has been fabricated with an excellent current sensitivity of 0.533 μA pM<sup>-1</sup> cm<sup>-2</sup> and a very low detection limit of 27.7 pM. The fabricated sensor shows exceptional selectivity to H<sub>2</sub>O<sub>2</sub> in the presence of high concentration of some likely interference. Moreover, the sensor exhibits high stability with appreciable repeatability and reproducibility.

Keywords: GO-CNT nanocomposite, direct electrochemistry, cytochrome *c*, hydrogen peroxide sensor, electrocatalysis

## 1. Introduction

Graphene oxide (GO) and its nanocomposites are rapidly emerging as very promising functional nanomaterials because of their facile synthesis, ease of processing and desirable physicochemical properties.<sup>1-3</sup> Especially, GO-based nanocomposites have been receiving a lot of attention for use in bioelectrochemical applications as they can provide a hydrophilic and biocompatible microenvironment required for the facile immobilization of various electroactive biomolecules and enzymes.<sup>4-6</sup> Functional GO in combination with metal / metal oxide nanoparticles have been applied in electrochemical sensing, electrocatalysis, fuel cells and supercapacitors.<sup>7-11</sup> Hybrid materials synthesized by the functionalization of GO with a variety of organic molecules have been reported to exhibit better electrochemical properties.<sup>12,13</sup> The excellent biocompatibility of GO-based electrodes makes them amenable for use in electrochemical biosensors. Several reports have already appeared in literature on the application of GO nanocomposites in DNA and heme protein biosensors.<sup>14, 15</sup>

GO-carbon nanotube (CNT) composites form relatively a new class of hybrid nanomaterials.<sup>16, 17</sup> The earlier studies were focused mainly on the use of GO for preparing homogeneous dispersion of CNTs in both aqueous and nonaqueous media.<sup>18-21</sup> The pioneering work by Cai et al<sup>22</sup> demonstrated the importance of GO-CNT mixing ratio in controlling the resistance and morphology of the resulting hybrid material. Recently, several reports have appeared in literature on the fabrication of the GO-CNT hybrid films by adopting various strategies including self-assembly,<sup>23, 24</sup> Langmuir-Blodgett assembly,<sup>25</sup> and electrostatic interaction.<sup>26</sup> A simple coagulation spinning technique has been used to prepare high strength fibres of the GO-CNT nanocomposite.<sup>27</sup> Very recently this novel material has been utilized in various electrochemical applications including supercapacitors, batteries, sensors and biosensors.<sup>28-33</sup> These studies have demonstrated the superior performance of

the nanocomposite as an electrode modifier in comparison to the CNT modified surface.

The electrochemical reduction of  $\text{H}_2\text{O}_2$  can be accomplished through direct electron transfer between the electrode and immobilized *horse radish peroxidase* enzyme<sup>34,35</sup> Alternatively, proteins such as haemoglobin, myoglobin and cytochrome *c* (Cyt *c*) containing heme groups, due to their peroxidase like catalytic activity can be used to construct  $\text{H}_2\text{O}_2$  biosensors.<sup>36-38</sup> However, a major challenge in such heme modified electrodes is that the direct electron transfer between the heme protein and electrode is often not very effective as the redox sites are deeply buried into bulk protein chains. Also the protein can get irreversibly denatured because of its unfavourable orientation to the bare electrode.<sup>39</sup> Thus, it is necessary to search for ways to develop new heme-modified electrodes with well- behaved electrochemistry and good stability.

Herein we report the direct electrochemistry of Cyt *c* immobilized onto the GO-CNT composite and its peroxidase like catalytic activity for the reduction of  $\text{H}_2\text{O}_2$ . The presence of GO in the nanocomposite provides a hydrophilic and biocompatible environment for the effective immobilization of Cyt *c*. On the other hand the high conducting network of CNT helps to achieve the direct electron transfer between Cyt *c* and the electrode. The highly efficient direct electron transfer of the Cyt *c* immobilized GO-CNT actually aids in the picomolar detection of  $\text{H}_2\text{O}_2$  with a remarkable current sensitivity. Such a trace level detection of  $\text{H}_2\text{O}_2$  is of prime importance in the fields of bio-imaging, healthcare and terrorism management.<sup>40-44</sup>

## 2. Experimental

### 2.1 Materials and methods

Cytochrome *c* from horse heart, graphite (powder, <20  $\mu\text{m}$ ), multi-walled carbon

nanotube (MWCNT), potassium tetrachloro aurate, nafion (Nf) 5 wt % were purchased from Sigma-Aldrich and used as received. 0.5 % Nf solution was prepared in ethanol. All reagents were of analytical grade and used as received without any further purification. 0.1 M phosphate buffer solutions (PBS) of pH varying from 1 to 11 were prepared by mixing standard stock solutions of  $\text{Na}_2\text{HPO}_4$  and  $\text{NaH}_2\text{PO}_4$  and adjusting the pH by the addition of either 0.1 M  $\text{H}_3\text{PO}_4$  or 0.1 M NaOH. Prior to each electrochemical experiment, all the solutions were deoxygenated with extra pure  $\text{N}_2$  gas for about 15 minutes.

The electrochemical measurements were carried out using CHI 611A workstation. A conventional three electrode cell using a glassy carbon electrode (GCE) as the working electrode (area  $0.07 \text{ cm}^2$ ), saturated Ag/AgCl as reference electrode and Pt wire as counter electrode was used. Amperometric measurements were performed by an analytical rotator AFMSRX (PINE instruments, USA) with a rotating disc electrode (RDE) having a working area of  $0.24 \text{ cm}^2$ . EIM6ex ZAHNER (Kroanch, Germany) was used for electrochemical impedance spectroscopy (EIS) studies using a frequency range between 100 mHz and 10 kHz at an applied AC voltage of 0.01 V. The morphology and surface topography were examined by a scanning electron microscope (SEM) (VEGA 3 SBU) and an atomic force microscope (AFM) (APE Research Model A100 SGS) respectively.

## 2.2 Preparation of GO-MWCNT composite

The GO-MWCNT composite was prepared as follows. Graphite oxide prepared by modified Hummer's method<sup>45</sup> was ultrasonically exfoliated for 2 h to get GO. About 5 mg of MWCNT was added to 10 mL of an aqueous dispersion of GO ( $0.5 \text{ mg mL}^{-1}$ ) and the mixture was subjected to ultrasonication for 2 h to obtain the GO-MWCNT composite. After the removal of undispersed MWCNT and GO by centrifugation, the GO-MWCNT composite

was washed in water and dried in oven for whole night and redispersed in water (0.5 mg mL<sup>-1</sup>). For parallel comparison studies, pristine GO and MWCNT dispersions (0.5 mg mL<sup>-1</sup>) were prepared in water and DMF solvents, respectively.

### 2.3 Fabrication of Nf/Cyt *c* /GO-MWCNT/AuNP/GCE modified electrode

The Cyt *c* immobilized GO-MWCNT bionanocomposite was formed on a nano Au modified glassy carbon electrode. Au nanoparticles modified GCE (AuNP/GCE) was prepared by cyclic voltammetric deposition in 0.1 M NaNO<sub>3</sub> aqueous solution containing 0.25 mM KAuCl<sub>4</sub> in the potential range between 0 and +0.9 V at a scan rate of 0.05 V s<sup>-1</sup> for 6 cycles. The resulting electrode was rinsed in water. Then the as prepared GO-MWCNT composite (6 μL) was drop coated onto this and dried for 10 min at room temperature to obtain GO-MWCNT/AuNP/GCE. Thereafter, 6 μL of Cyt *c* (10 mg mL<sup>-1</sup> of PBS pH 7) was drop coated onto this and after a standing time of about 30 minutes, the Cyt *c*/GO-MWCNT/AuNP/GCE electrode was carefully rinsed with water to remove the unadsorbed Cyt *c* and then dried. At the end, 2 μL of 0.5% Nf was drop coated onto the enzyme modified electrode and dried at room temperature to get the Nf/Cyt *c*/GO-MWCNT/AuNP/GCE modified electrode. The Nf coating onto the composite film is expected to prevent the leakage of Cyt *c* from the electrode matrix and thereby improve the stability of the composite film.<sup>46</sup> For comparison Nf/Cyt *c*/GCE, Nf/Cyt *c*/GO/AuNP/GCE, and Nf/Cyt *c*/MWCNT/AuNP/GCE modified electrodes were also prepared.

## 3. Results and discussion

### 3.1 Morphological and surface characterization

Fig. 1A is the scanning electron microscopy image obtained for the GO-MWCNT/AuNP film which shows the presence of interconnected MWCNTs in tight contact with the GO surface, suggesting a strong interaction between them. The image conveys the presence of a highly percolating porous morphology which will be greatly suitable for enzyme immobilization. The SEM image of the Cyt *c* immobilized GO-MWCNT/AuNP shown in Fig. 1B is rather different from that before immobilization in that it shows a compact morphology. Typical 2D and 3D AFM images of the GO-MWCNT/AuNP films before and after Cyt *c* immobilization are shown in Figs. 1C to 1F. The AFM images before immobilization (1C & 1D) show the presence of non-agglomerated bundles of MWCNTs uniformly dispersed on the GO surface while those after immobilization (1E & 1F) clearly show that the protein molecules densely cover the entire surface of the GO-MWCNT composite film. The height difference between the two films is found to be about 12 nm indicating a multi-layer coverage by Cyt *c*.

### [Figure 1]

### 3.2 Electrochemical impedance spectroscopy (EIS) studies

EIS is a powerful method to characterize the electrical properties of the materials and to monitor the changes associated with interfacial properties and thereby allowing to understand the chemical transformation and processes associated with the conductive electrode surface.<sup>47</sup> Therefore, in the present study, the EIS technique is applied to derive information about the impedance changes at the electrode/electrolyte interface arising out of electrode modification. All the EIS experiments were performed in an electrolyte solution consisting of an equimolar mixture 5 mM  $\text{Fe}(\text{CN})_6^{3-}/\text{Fe}(\text{CN})_6^{4-}$  in 0.1 M KCl. Fig. 2A shows the complex impedance spectra represented as Nyquist plots ( $Z'$  vs.  $Z''$ ) for (a) bare GCE,

(b) Nf/Cyt *c*/GCE, (c) AuNP/GCE, (d) GO-MWCNT/AuNP/GCE, and (e) Nf/Cyt *c*/GO-MWCNT/AuNP/GCE. The impedance data could be fitted to the Randles circuit shown in the inset of Fig.2, where  $R_s$  is electrolyte resistance,  $R_{ct}$  is charge transfer resistance,  $C_{dl}$  is double layer capacitance and  $Z_w$  is Warburg impedance. In the Randles circuit, the  $R_{ct}$  and Warburg impedance can be found to be parallel to  $C_{dl}$  which results in a semicircle in the Nyquist plots. The diameter of the semicircle is equal to the  $R_{ct}$  value which is indicative of the electron transfer kinetics of the redox probe at the electrode/electrolyte interface. The Nyquist plot of bare GCE exhibits a large semicircle with an  $R_{ct}$  value of 641  $\Omega$ . The  $R_{ct}$  value of Cyt *c* /GCE (785  $\Omega$ ) is slightly increased compared to bare GCE which is caused by the nonconductive properties of the biomacromolecule. The AuNP/GCE shows a smaller semicircle than that observed at bare GCE, indicating that the  $R_{ct}$  value (84  $\Omega$ ) has been substantially reduced compared to bare GCE after the deposition of Au nanoparticles. The GO-MWCNT/AuNP/GCE displays almost a similar behaviour with even more reduced  $R_{ct}$  of 10  $\Omega$  implying that the GO-MWCNT/AuNP/GCE composite provides an excellent conducting surface with accelerated electron transfer. The  $R_{ct}$  value of Nf/Cyt *c*/GO-MWCNT/AuNP/GCE is increased from 10  $\Omega$  to 24  $\Omega$  suggesting that Cyt *c* enzyme is successfully immobilized onto the modified electrode surface.

[Figure 2]

### 3.3 Direct electrochemistry of Cyt *c* at the Nf /Cyt *c*/GO-CNT/AuNP modified GCE

Fig. 2B shows the background cyclic voltammograms (CVs) of (a) Nf/Cyt *c*/GCE, (b) Nf/Cyt *c*/GO-MWCNT/AuNP/GCE, (c) Nf/Cyt *c*/MWCNT/AuNP/GCE, (d) Nf/Cyt *c*/GO/AuNP/GCE in PBS (pH 7) at a scan rate of 0.05 V s<sup>-1</sup>. The CV of Nf/Cyt *c*/GCE shows a cathodic peak at -0.36 V with a less prominent anodic peak at about -0.26 V corresponding to the Fe<sup>III/II</sup> redox couple of Cyt *c*. The very low current magnitudes of 0.5

$\mu\text{A}$  for  $I_{pc}$  and  $0.1 \mu\text{A}$  for  $I_{pa}$  arise due to its large  $R_{ct}$  value. The CV of Nf/Cyt *c*/GO-MWCNT/AuNP/GCE modified electrode shows well defined redox peaks ( $E_{pa}$  at  $-0.34 \text{ V}$  and  $E_{pc}$  at  $-0.28 \text{ V}$ ) for the  $\text{Fe}^{\text{III/II}}$  redox couple of Cyt *c* with a peak to peak separation value of ( $\Delta E_p$ )  $-0.06 \text{ V}$  corresponding to a  $1e$  reversible process. The peak current magnitudes ( $I_{pc} = 6.1 \mu\text{A}$  ;  $I_{pa} = 4.1 \mu\text{A}$ ) are also found to be substantially improved compared to those of Nf/Cyt *c*/GCE. In order to bring out the role of GO and MWCNT in the direct electrochemistry of Cyt *c*, the background CVs have been obtained with Nf/Cyt *c*/MWCNT/AuNP/GCE and Nf/Cyt *c*/GO/AuNP/GCE as well. The CV of Nf/Cyt *c*/MWCNT/AuNP/GCE shows a pair of redox peaks with  $E_{pa}$  and  $E_{pc}$  at  $-0.33$  and  $-0.25 \text{ V}$  respectively with a  $\Delta E_p$  of  $-0.08 \text{ V}$  indicating that the direct electron transfer can also be observed at this modified electrode. However, the peak current values ( $I_{pc} = 1.6 \mu\text{A}$  ;  $I_{pa} = 0.8 \mu\text{A}$ ) are much lower than those observed at the Nf/Cyt *c*/GO-MWCNT/AuNP/GCE modified electrode. On the other hand, the CV of Nf/Cyt *c*/GO/AuNP/GCE does not show any characteristic redox process corresponding to the Cyt *c* suggesting that the direct electrochemistry has not been achieved at this electrode. This is perhaps due to the poor conductivity of the electrode. A comparison of  $\Delta E_p$  and the ratio of peak currents between Nf/Cyt *c*/MWCNT/AuNP/GCE and Nf/Cyt *c*/GO-MWCNT/AuNP/GCE suggests that the kinetics of the direct electrochemistry of Cyt *c* is rather faster at the latter electrode.

### 3.4. Effect of scan rate

The effect of scan rate on the Cyt *c* redox process at the Nf/Cyt *c*/GO-MWCNT/AuNP/GCE electrode is examined in PBS (pH 7). Fig. 3A displays the CVs of the immobilized Cyt *c* at various scan rates from  $0.05$  to  $1 \text{ V s}^{-1}$ . It can be observed that the cathodic and anodic redox peak currents of Cyt *c* are increased linearly with increase in scan

rate (inset of Fig. 3A) indicating that the redox process occurring at the Nf/Cyt *c*/GO-MWCNT/AuNP/GCE electrode is a surface-controlled electrode process and also confirming that the immobilized state of Cyt *c* is stable at all scan rates. Also, with increase in scan rates, the oxidation peak shifts to more positive potentials, while the reduction peak shifts to more negative potentials. The anodic ( $E_{pa}$ ) and cathodic ( $E_{pc}$ ) peak potentials are plotted against the logarithm of scan rate. Applying Laviron theory,<sup>48</sup> the charge transfer coefficient can be calculated for a surface controlled process using eqn (1).

$$\frac{k_a}{k_c} = \frac{\alpha}{(1-\alpha)} \quad (1)$$

where  $k_a$  is the slope of the linear plot of  $E_{pa}$  vs  $\log v$  (0.069) and  $k_c$  is the slope of the linear plot of  $E_{pc}$  vs  $\log v$  (0.091) and  $\alpha$  is the charge-transfer coefficient which is calculated to be 0.43. The apparent electron transfer rate constant ( $k_s$ ) can be obtained using eqn (2).

$$\log k_s = \alpha \log (1-\alpha) + (1-\alpha) \log \alpha - \log \frac{RT}{nFv} - \frac{\alpha(1-\alpha) nF\Delta E_p}{2.3 RT} \quad (2)$$

The obtained  $k_s$  value of  $3.4 \text{ s}^{-1}$  for the Nf/Cyt *c*/GO-MWCNT/AuNP/GCE electrode is found to be higher than that of Cyt *c*/L-cysteine modified electrode ( $0.28 \text{ s}^{-1}$ ),<sup>36</sup> Cyt *c* immobilized colloidal Au modified carbon paste electrode ( $1.21 \text{ s}^{-1}$ )<sup>49</sup> and Cyt *c* adsorbed amine functionalized silica thin films ( $1.33 \text{ s}^{-1}$ ).<sup>50</sup> This result reveals that the GO-MWCNT nanocomposite is an excellent biocompatible material for the electron transfer of Cyt *c*.

The surface concentration of the Cyt *c* molecules at the Nf/Cyt *c*/GO-MWCNT/AuNP/GCE electrode has been estimated based on the slope of  $I_p$  vs  $v$  plot using the Laviron equation eqn (3):<sup>51</sup>

$$I_p = \frac{n^2 F^2 A \nu \Gamma}{4RT} \quad (3)$$

where  $n$ ,  $I_p$ ,  $A$ ,  $\nu$  and  $\Gamma$  represent the number of electrons transferred in the redox reaction ( $n=1$ ),  $I_p$  is the reduction peak current,  $A$  represents geometric area of the electrode ( $\text{cm}^2$ ),  $\nu$  is the scan rate ( $\text{V s}^{-1}$ ) and  $\Gamma$  is the surface coverage concentration of enzyme on the electrode surface ( $\text{mol cm}^{-2}$ ) respectively. The constants  $F$ ,  $R$  and  $T$  represent Faraday constant ( $96485 \text{ C mol}^{-1}$ ), gas constant ( $8.314 \text{ J K}^{-1} \text{ mol}^{-1}$ ) and temperature ( $298 \text{ K}$ ) respectively. By substituting all the known values in eqn (3), the surface coverage of enzyme Cyt  $c$  at the GO-MWCNT/AuNP/GCE is calculated to be  $1.82 \times 10^{-9} \text{ mol cm}^{-2}$ , which is higher than the theoretical monolayer coverage of  $1.4 \times 10^{-12} \text{ mol cm}^{-2}$ .<sup>52</sup> Therefore it is inferred that the nanocomposite electrode GO-MWCNT/AuNP/GCE possesses a large number of active sites on its surface facilitating the immobilization of Cyt  $c$  to a greater extent.

### [Figure 3]

#### 3.5. Effect of pH

In order to study the influence of pH on the electrochemical properties of the Nf/Cyt  $c$ /GO-MWCNT/AuNP/GCE modified electrode, CVs were recorded in aqueous buffer solutions of various pH in the range between 1 and 11 at a scan rate of  $0.05 \text{ V s}^{-1}$  which are shown in Fig. 3B. The results show that the formal potential ( $E^0$ ) of the redox couple responsible for the direct electrochemistry of Cyt  $c$  shifts negatively with increase in pH. A plot of formal potential against pH is linear as exemplified in the inset to Fig. 3B, which indicates that the electron transfer between the immobilized Cyt  $c$  and the electrode is accompanied by proton transfer. The obtained slope value of  $-0.033 \text{ V/pH}$  is less than the expected value of  $-0.059 \text{ V/pH}$  for a reversible single electron transfer coupled with a proton. Such a lower slope value was reported for many other heme protein modified electrodes

and was attributed to the influence of the protonation states of trans ligands to the heme iron and amino acids around the heme<sup>53</sup> or to the protonation of the water molecules coordinated to the central iron atom.<sup>54</sup>

### 3.6. Electrocatalytic reduction of H<sub>2</sub>O<sub>2</sub> at Nf/Cyt *c*/GO-MWCNT/AuNP/GCE

The electrocatalytic ability of the Nf/Cyt *c*/GO-MWCNT/AuNP/GCE towards the reduction of H<sub>2</sub>O<sub>2</sub> was investigated by cyclic voltammetry. Fig. 4A displays the CVs of Nf/Cyt *c*/GO-MWCNT/AuNP/GCE modified electrode in PBS of pH 7 with increasing concentration of H<sub>2</sub>O<sub>2</sub> from 0.2 to 2.4 mM (b to l). Curve a in the Fig. 4A shows the background CV of the Nf/Cyt *c*/GO-MWCNT/AuNP/GCE electrode without any addition of H<sub>2</sub>O<sub>2</sub>. From these results, it can be noted that in the absence of H<sub>2</sub>O<sub>2</sub>, only the redox peaks of the immobilized Cyt *c* are observed. Upon an addition of 0.2 mM of H<sub>2</sub>O<sub>2</sub>, the cyclic voltammogram shows an increase of reduction peak current and decrease of oxidation peak current. Further additions of H<sub>2</sub>O<sub>2</sub> increased the reduction peak current with concurrent decrease of the oxidation peak current. These results clearly demonstrate the excellent electrocatalytic ability of the Nf/Cyt *c*/GO-MWCNT/AuNP/GCE towards the reduction of H<sub>2</sub>O<sub>2</sub>. The negligible oxidation peak current shows that the oxidation rate of Cyt *c* by H<sub>2</sub>O<sub>2</sub> is very fast, indicating the pseudo peroxidase activity of the Cyt *c* immobilized onto the GO-MWCNT composite. The electrocatalytic process can be described by eqn (4) and eqn (5).<sup>55</sup>

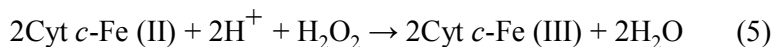
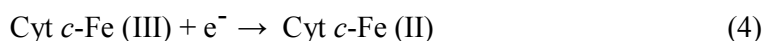


Fig 4B shows the CVs of Nf/Cyt *c*/GO-MWCNT/AuNP/GCE film modified electrode in PBS of pH 7 containing 1 mM of H<sub>2</sub>O<sub>2</sub> at different scan rates from 0.1 to 1 V s<sup>-1</sup> (a to j). The reduction peak current increases linearly with increase in scan rate. A plot of the

reduction peak current against the scan rate exhibits a linear relationship and this indicates that the reduction of  $\text{H}_2\text{O}_2$  is a diffusion-controlled process.

[Figure 4]

### 3.7. Amperometric determination of $\text{H}_2\text{O}_2$

Owing to the excellent electrocatalytic ability of the Nf/Cyt *c*/GO-MWCNT/AuNP/GCE towards  $\text{H}_2\text{O}_2$ , an amperometric sensor has been constructed for the trace level detection of  $\text{H}_2\text{O}_2$ . Fig 5A shows the amperometric response for each addition of 10 pM concentration of  $\text{H}_2\text{O}_2$  at a regular interval of 50 s into deaerated PBS (pH 7) at an applied potential of -0.2 V and an electrode rotation speed of 1000 rpm. The amperometric response current increases linearly with increasing  $\text{H}_2\text{O}_2$  concentration from 10 to 140 pM. For every addition of  $\text{H}_2\text{O}_2$ , the steady state current is reached within 6 s, indicating that the sensor has a short response time. The corresponding calibration curve of the fabricated amperometric  $\text{H}_2\text{O}_2$  sensor (Inset (bottom) of Fig. 5A) exhibits a linear response with a correlation coefficient of 0.981 and the linear equation can be represented as  $I (\mu\text{A}) = 0.128 [\text{H}_2\text{O}_2] (\text{pM}) + 3.875$ . The limit of detection (LOD) was estimated using the formula in eqn (6):<sup>56</sup>

$$\text{LOD} = 3 s_b/m \quad (6)$$

where  $s_b$  is the standard deviation obtained from five measurements of the blank signal i.e. 1.182  $\mu\text{A}$  and  $m$  is the analytical sensitivity represented by the slope of the calibration plot (0.128  $\mu\text{A}/\text{pM}$ ). From these data, the LOD is estimated to be 27.7 pM with a signal-to-noise ratio of 7 (Inset (top) of Fig. 5A) and the sensitivity value is determined to be 0.533  $\mu\text{A pM}^{-1} \text{cm}^{-2}$ .

It may be mentioned here that the H<sub>2</sub>O<sub>2</sub> sensor performance of the Cyt *c* immobilized GO-MWCNT nanocomposite based electrode is found to be superior to the other reported Cyt *c* immobilized modified electrode based biosensors in terms of LOD and current sensitivity as can be seen from Table 1<sup>,57-63</sup>.

[Figure 5]

### 3.8. Interference Studies

The selectivity of the proposed biosensor was investigated in the presence of some potentially coexisting interference substances such as uric acid (UA), ascorbic acid (AA), dopamine (DA) and glucose (Glu) in biological systems. Fig. 5B shows the amperometric responses of Nf/Cyt *c*/GO-MWCNT/AuNP modified GCE for the consecutive additions of (a) 10 pM H<sub>2</sub>O<sub>2</sub>, (b) 1 μM DA, (c) 1 μM AA, (d) 1 μM UA and (e) 1 μM Glu at a regular interval of 50 s to PBS of pH 7. At first the nanocomposite bioelectrode showed well defined amperometric responses for the addition of 10 pM H<sub>2</sub>O<sub>2</sub>. It is found from the results that dopamine, ascorbic acid, uric acid, and glucose have very low interference effect (< 2%) on H<sub>2</sub>O<sub>2</sub> determination. Thus the fabricated Nf/Cyt *c*/GO-MWCNT/AuNP nanocomposite based sensor exhibits a versatile ability to be devoid of being influenced by such possible interferences coexisting along with H<sub>2</sub>O<sub>2</sub>.

### 3.9. Stability, repeatability and reproducibility studies

The stability of the Nf/Cyt *c*/GO-MWCNT/AuNP nanocomposite electrode was investigated by recording 100 consecutive cyclic voltammograms in PBS of pH 7 at a scan rate of 0.05 V s<sup>-1</sup>. It was calculated that about 92% of both the initial cathodic and anodic currents were retained in the 100<sup>th</sup> cycle, showing that the modified film was highly stable and the immobilised Cyt *c* was tightly anchored to the modified film. In addition, we

found that the nanocomposite electrode retains its 95 % (both  $I_{pa}$  and  $I_{pc}$ ) of the initial current after one month of its storage under 4 °C in refrigerator. Thus, the fabricated sensor possesses excellent stability due to the strong affinity between Cyt *c* and GO-MWCNT composite.

The repeatability and reproducibility of the fabricated biosensor was studied by performing cyclic voltammetry in PBS of pH 7 at a scan rate of 0.05 V s<sup>-1</sup>. The sensor exhibits acceptable reproducibility with a relative standard deviation (R.S.D) of 2.3 % for 15 individual measurements and a repeatability of 5.3 % for 10 successive measurements. Thus the Nf/Cyt *c*/GO-MWCNT/AuNP/GCE exhibits acceptable repeatability and reproducibility results.

#### [Table 1]

#### 4. Conclusions

We fabricated a simple H<sub>2</sub>O<sub>2</sub> biosensor based on Nf/Cyt *c*/GO-MWCNT/AuNP/GCE for the picomolar level detection of H<sub>2</sub>O<sub>2</sub>. The presence of GO in the electrode matrix greatly eases the immobilization of Cyt *c* with a surface coverage value of 1.82×10<sup>-9</sup> mol cm<sup>-2</sup>. Cyclic voltammetry data clearly demonstrate the direct electrochemistry of Cyt *c* at this nanocomposite electrode. Moreover the large  $k_s$  value obtained for the redox process shows that the composite film modified electrode significantly enhances the electrical communication between the Cyt *c* and the electrode surface. The fabricated amperometric sensor exhibits excellent performance with a high sensitivity of 0.533 μA pM<sup>-1</sup> cm<sup>2</sup> and very low detection limit of 27.7 pM.

## Acknowledgements

This work was supported by Indo-Taiwan exchange programme, Department of Science and Technology, New Delhi and National Science Council and Ministry of Education of Taiwan (Republic of China). Bose Dinesh gratefully acknowledges University Grants Commission for a Meritorious Fellowship.

## References

- [1] D. Chen, H. Feng, J. Li, *Chem. Rev.*, 2012, **112**, 6027-6053.
- [2] B.G. Eda, M. Chhowalla, *Adv. Mater.*, 2010, **22**, 2392-2415.
- [3] D.R. Dreyer, S. Park, C.W. Bielawski, R.S. Ruoff, *Chem. Soc. Rev.*, 2010, **39**, 228-240.
- [4] S. Uhm, H. Tuyen, J. Lee, *Electrochem. Commun.*, 2011, **13**, 677-680.
- [5] B. Yuan, X. Zeng, C. Xu, L. Liu, Y. Ma, D. Zhang, Y. Fanc, *Sens. Actuators, B*, 2013, **184**, 15-20.
- [6] X. Zuo, S. He, D. Li, C. Peng, Q. Huang, S. Song, C. Fan, *Langmuir*, 2010, **26**, 1936-1939.
- [7] S. Chen, J. Zhu, X. Wu, Q. X. Han, X. Wang, *ACS Nano*, 2010, **4**, 2822-2830.
- [8] Y. Cui, Q-Y. Cheng, H. Wu, Z. Wei, B-H. Han, *Nanoscale*, 2013, **5**, 8367-8374.
- [9] C-T. Hsieh, W-Y. Chen, D-Y. Tzou, A.K. Roy, H-T. Hsiao, *Int. J. Hydrogen Energy*, 2012, **37**, 17837-17843.
- [10] G-H. Wu, Y-F. Wu, X-W. Liu, M-C. Rong, X-M. Chen, X. Chen, *Anal. Chim. Acta*, 2012, **745**, 33-37.
- [11] H. Xiong, B. Jin, *J. Electroanal. Chem.*, 2011, **661**, 77-83.
- [12] N. Karousis, S.P. Economopoulos, E. Sarantopoulou, N. Tagmatarchis, *Carbon*, 2010, **4**, 854-860.
- [13] A. Österholm, T. Lindfors, J. Kauppila, P. Damlinb, C. Kvarnström, *Electrochim. Acta*, 2012, **83**, 463-470.
- [14] A. Erdem, M. Muti, P. Papakonstantinou, E. Canavar, H. Karadeniz, G. Congur, S. Sharma, *Analyst*, 2012, **137**, 2129-2135.
- [15] C. Guo, H. Sun, X.S. Zhao, *Sens. Actuators, B*, 2012, **164**, 82-89.
- [16] H.X. Kong, *Curr. Opin. Solid State Mater. Sci.*, 2013, **17**, 31-37.
- [17] V. Mani, B. Devadas, S-M. Chen, *Int. J. Electrochem. Sci.*, 2013, **8**, 11641 - 11660.
- [18] X. Dong, G. Xing, M.P.C. Park, W. Shi, N. Xiao, *Carbon*, 2011, **49**, 5071-5078.

- [19] L. Qiu, X. Yang, X. Gou, W. Yang, Z-F. Ma, G.G. Wallace, D. Li, *Chem. -Eur. J.*, 2010, **16**, 10653-10658.
- [20] L. Tian, M.J. Meziani, F. Lu, C.Y. Kong, L. Cao, T.J. Thorne, Y-P. Sun, *ACS Appl. Mater. Interfaces*, 2010, **2**, 3217-3222.
- [21] C. Zhang, L. Ren, X. Wan, T. Liu, *J. Phys. Chem. C*, 2010, **114**, 11435-11440.
- [22] B.D. Cai, M. Song, C. Xu, *Adv. Mater.*, 2008, **20**, 1706-1709.
- [23] J.J. Shao, W. Lv, Q. Guo, C. Zhang, Q. Xu, Q-H. Yang, F. Kang, *Chem. Commun.*, 2012, **48**, 3706-3708.
- [24] Q. Zhang, S. Yang, J. Zhang, L. Zhang, P. Kang, J. Li, J. Xu, H. Zhou, X-M. Song, *Nanotech.*, 2011, **22**, 494010-494017.
- [25] Q. Zhang, B. Zhang, X. Lin, N. Yousefi, Z-D. Huang, Z. Li, J-K. Kim, *J. Mater. Chem.*, 2012, **22**, 25072-25082.
- [26] Y.K. Kim, H.K. Na, S.J. Kwack, S.R. Ryoo, Y. Lee, S. Hong, S. Hong, Y. Jeong, D-H. Min, *ACS Nano*, 2011, **5**, 4550-4561.
- [27] R. Wang, J. Sun, G. Lian, C. Xu, J. Zhang, *Chem. Commun.*, 2011, **47**, 8650-8652.
- [28] S. Cheemalapati, S. Palanisamy, V. Mani, S-M.Chen, *Talanta*, 2013, **117**, 297-304.
- [29] J. Li, D. Kuang, Y. Feng, F. Zhang, Z. Xu, M. Liu, D. Wang, *Microchim. Acta*, 2013, **180**, 49-58.
- [30] L-Y. Lin, M-H. Yeh, J-T. Tsai, Y-H. Huang, C-L. Sun, K-C. Ho, *J. Mater. Chem. A*, 2013, **1**, 11237-11245.
- [31] S. Luo, Y. Wu, H. Gou, *Ionics*, 2013, **19**, 673-680.
- [32] C. Wu, X. Huang, X. Wu, L. Xie, K. Yang, P. Jiang, *Nanoscale*, 2013, **5**, 3847-3855.
- [33] K. Zhang, L. Lu, Y. Wen, J. Xu, X. Duan, L. Zhang, D. Hu, T. Nie, *Anal. Chim. Acta*, 2013, **787**, 50-56.
- [34] Q. Wang, A. Kromka, J. Houdkova, O. Babchenko, B. Rezek, M. Li, R. Boukherroub, S. Szunerits, *Langmuir*, 2012, **28**, 587-592.

- [35] A.J. Saleh-Ahmed, *J. Biosens. Bioelectron.*, 2013, doi: 10.4172/2155-6210.S9-001.
- [36] Y-C. Liu, S-Q. Cui, J. Zhao, Z-S. Yang, *Bioelectrochem.*, 2007, **7**, 416-420.
- [37] M. Wang, Q. Sheng, D. Zhang, Y. He, J. Zheng, *Bioelectrochem.*, 2012, **86**, 46-53.
- [38] L. Xie, Y. Xu, X. Cao, *Colloids Surf.*, 2013, **107**, 245-250.
- [39] J.J. Feng, G. Zhao, J.J. Xu, Y.H. Chen, *Anal. Biochem.*, 2005, **342**, 280-286.
- [40] J. Benedet, D. Lu, K. Cizek, J.L. Belle, J. Wang, *Anal. Bioanal. Chem.*, 2009, **395**, 371-376.
- [41] R. Chen, L. Zhang, G. Gao, W. Wu, Y. Hu, X. Jiang, *J. Biomed. Biotech.*, **2011**, Article ID 679492.
- [42] D. Lee, S.J.C. Khaja, J.C. Velasquez-Castano, M. Dasari, C. Sun, J. Petros, W.R. Taylor, N. Murthy, *Nat. Mater.*, 2007, **6**, 765-769.
- [43] R. Schulte-Ladbeck, M. Vogel, U. Karst, *Anal. Bioanal. Chem.*, 2006, **386**, 559-565.
- [44] R. Stolarek, P. Bialasiewicz, M. Krol, D. Nowak, *Clin. Chim. Acta*, 2010, **411**, 1849-1861.
- [45] W.S. Hummers, R.E. Offeman, *J. Am. Chem. Soc.*, 1958, **80**, 1339.
- [46] C. Guo, H. Sun, X.S. Zhao, *Sens. Actuators, B*, 2012, **164**, 82-89.
- [47] F. Lisdat, D. Schafer, *Anal. Bioanal. Chem.*, 2008, **391**, 1555-1567.
- [48] E. Laviron, *J. Electroanal. Chem.*, 1979, **101**, 9-28.
- [49] H.X. Ju, Q.S. Liu, X.B. Ge, F. Lisdat, W.F. Scheller, *Electroanal.*, 2002, **14**, 141-147.
- [50] X. Zhang, J. Wang, W. Wu, S. Qian, Y. Man, *Electrochem. Commun.*, 2007, **9**, 2098-2104.
- [51] A.J. Bard, R.L. Faulkner, *Wiley*, New York, 2001.
- [52] R.E. Dickerson, T. Takano, D. Eisenberg, O.B. Kallai, L. Samson, A. Cooper, E. Margoliash, *J. Biol. Chem.*, 1971, **246**, 1511-1535.
- [53] J.J. Feng, G. Zhao, J.J. Xu, Y.H. Chen, *Anal. Biochem.*, 2005, **342**, 280-286.
- [54] J-Y. Sun, K-J. Huang, S-F. Zhao, Y. Fan, Z-W. Wu, *Bioelectrochem.*, 2011, **82**, 125-130.

- [55] A. K. Yagati, T. Lee, J. Min, J-W. Choi, *Colloids Surf., B*, **92**, 161-167.
- [56] G.L.Long, J.D.Winefordner, *Anal. Chem.*, 1983, **55**, 712 A.
- [57] N. Zhang, X. Lv, W. Ma, Y. Hu, F. Li, D. Han, L. Niu, *Talanta*, 2013, **107**, 195-202.
- [58] Z. Dai, S. Liu, H. Ju, *Electrochim Acta*, 2011, **28**, 210-215.
- [59] K-P Lee, A. I. Gopalan, S. Komathi, *Sens. Actuators, B*, 2009, **141**, 518-525.
- [60] A. Zhu, Y. Tian, H. Liu, Y. Luo, *Biomaterials*, 2009, **30**, 3183-3188.
- [61] M. Eguilaz, L. Agui, P. Yanez-Sedeno, J. M. Pingarron, *J. Electroanal. Chem.*, 2010, **644**, 30-35.
- [62] S. A. Kumar, S-F. Wang, C. T. Yeh, H. C. Lu, J. C. Yang, Y. T. Chang, *J. Solid State Electrochem*, 2010, **14**, 2129-2135.
- [63] G-X. Wang, Y. Qian, X. X. Cao, X-H. Xia, *Electrochem. Commun.*, 2012, **20**, 1-3.

**Table 1** Comparison of H<sub>2</sub>O<sub>2</sub> chronoamperometric sensor performance at Nf/Cyt *c*/GO-MWCNT/AuNP electrode with other Cyt *c* immobilized modified electrodes reported in literature

Electrode	Detection limit (nM)	Linear range (μM)	Sensitivity/ μA pM <sup>-1</sup> cm <sup>-2</sup>	Ref.
Cyt <i>c</i> /PTCA <sup>a</sup> -graphene/GCE	3500	5-90	2.44 x 10 <sup>-7</sup>	[57]
Cyt <i>c</i> /NaY <sup>b</sup> /GCE	320.0	8 - 128	2.02 x 10 <sup>-7</sup>	[58]
Cyt <i>c</i> /MWCNT-PANI <sup>c</sup> /ITO	300.0	0.5-1500	3.20 x 10 <sup>-8</sup>	[59]
Cyt <i>c</i> /nanoporous Au film	6300	10 -12000	2.80 x 10 <sup>-9</sup>	[60]
Cyt <i>c</i> / l-Cys <sup>d</sup> / P3MT <sup>e</sup> /MWCNT/GCE	230.0	0.7-400	-	[60]
Cyt <i>c</i> /MWCNTs/CF <sup>f</sup> /GCE	1000	2-78	-	[61]
Cyt <i>c</i> /Graphene-PEDOT <sup>g</sup> /GCE	249.0	0.5-400	-	[62]
Nf/Cyt <i>c</i> /GO-CNT/AuNP/GCE	0.027	1 x 10 <sup>-5</sup> – 1.4 x 10 <sup>-4</sup>	0.53	This work

a - perylene tetracarboxylic acid, b - Zeolite, c - Polyaniline, d - l-Cystine, e - P3MT-poly(-3 methylthiophene), f - ciprofloxacin, g - poly(3,4ethylenedioxythiophene)

**Figure Captions**

**Fig. 1** SEM images of (A) GO-MWCNT/Au film and (B) Cyt *c*/GO-MWCNT/Au film and 2D & 3D AFM images of GO-MWCNT/Au (C & D) and Cyt *c*/GO-MWCNT/Au film (E and F).

**Fig. 2** (A) EIS of various modified electrodes in 0.1 M KCl solution containing 5 mM  $\text{Fe}(\text{CN})_6^{3-/4-}$  at (a) bare GCE (b) Nf/Cyt *c*/GCE/ (c) AuNP/GCE (d) GO-MWCNT/AuNP/GCE and (e) Nf/Cyt *c*/GO-MWCNT/AuNP/GCE. Inset: Randles equivalent circuit model.

(B) Cyclic voltammograms at (a) Nf/Cyt *c*/GCE (b) Nf/Cyt *c*/GO-MWCNT/AuNP/GCE (c) Nf/Cyt *c*/MWCNT/AuNP/GCE (d) Nf/Cyt *c*/GO/AuNP/GCE in PBS (pH 7) at a scan rate of 0.05  $\text{V s}^{-1}$ .

**Fig. 3** (A) Cyclic voltammograms at Nf/Cyt *c*/GO-MWCNT/AuNP/GCE in PBS (pH 7) at different scan rates in  $\text{V s}^{-1}$  (a) 0.05, (b) 0.1, (c) 0.2, (d) 0.3, (e) 0.4, (f) 0.5, (g) 0.6, (h) 0.7, (i) 0.8, (j) 0.9 and (k) 1. Inset: Plot of anodic peak current ( $I_{pa}$ ) and cathodic peak current ( $I_{pc}$ ) against scan rate.

(B) Influence of pH on cyclic voltammograms at Nf/Cyt *c*/GO-MWCNT/AuNP/GCE in PBS of pH (a) 1 (b) 3 (c) 7 (d) 9 and (e) 11). Scan rate: 0.05  $\text{V s}^{-1}$ . Inset: Plot of formal potential ( $E^{\circ}$ ) against pH.

**Fig. 4** (A) Cyclic voltammograms at Nf/Cyt *c*/GO-MWCNT/AuNP/GCE in 0.1 M PBS (pH 7) (curve a) and in the presence of  $\text{H}_2\text{O}_2$  (b) 0.2 (c) 0.4 (c) 0.6 (d) 0.8 (e) 1 (f) 1.2 (g) 1.4 (h) 1.6 (i) 1.8 (j) 2 (k) 2.2 and (l) 2.4 mM. Inset: Plot of reduction peak current against  $\text{H}_2\text{O}_2$  concentration

(B) Cyclic voltammograms at Nf/Cyt *c*/GO-MWCNT/AuNP/GCE in PBS (pH 7) containing 1 mM  $\text{H}_2\text{O}_2$  at different scan rates in  $\text{V s}^{-1}$  (a) 0.1, (b) 0.2, (c) 0.3, (d) 0.4, (e) 0.5, (f) 0.6, (g) 0.7, (h) (i) 0.8, (j) 0.9 and (k) 1. Inset: Plot of  $\text{H}_2\text{O}_2$  reduction peak current against square root of scan rate.

**Fig. 5** (A) Chronoamperometric response at Nf/Cyt *c*/GO-MWCNT/AuNP with successive additions of 10 pM H<sub>2</sub>O<sub>2</sub> into a continuously stirred N<sub>2</sub> saturated PBS (pH 7). E<sub>app</sub>: - 0.2 V. Inset at the bottom: Calibration plot for the H<sub>2</sub>O<sub>2</sub> sensor. The upper inset shows the current response of the sensor toward the addition of 10 pM H<sub>2</sub>O<sub>2</sub> for evaluation of signal-to-noise ratio.

(B) Chronoamperometric response at Nf/Cyt *c*/GO-MWCNT/AuNP in 0.1 M PBS (pH 7) with 10 pM of H<sub>2</sub>O<sub>2</sub> and in the presence of 1 μM DA, AA, UA and Glu in E<sub>app</sub>: - 0.2 V

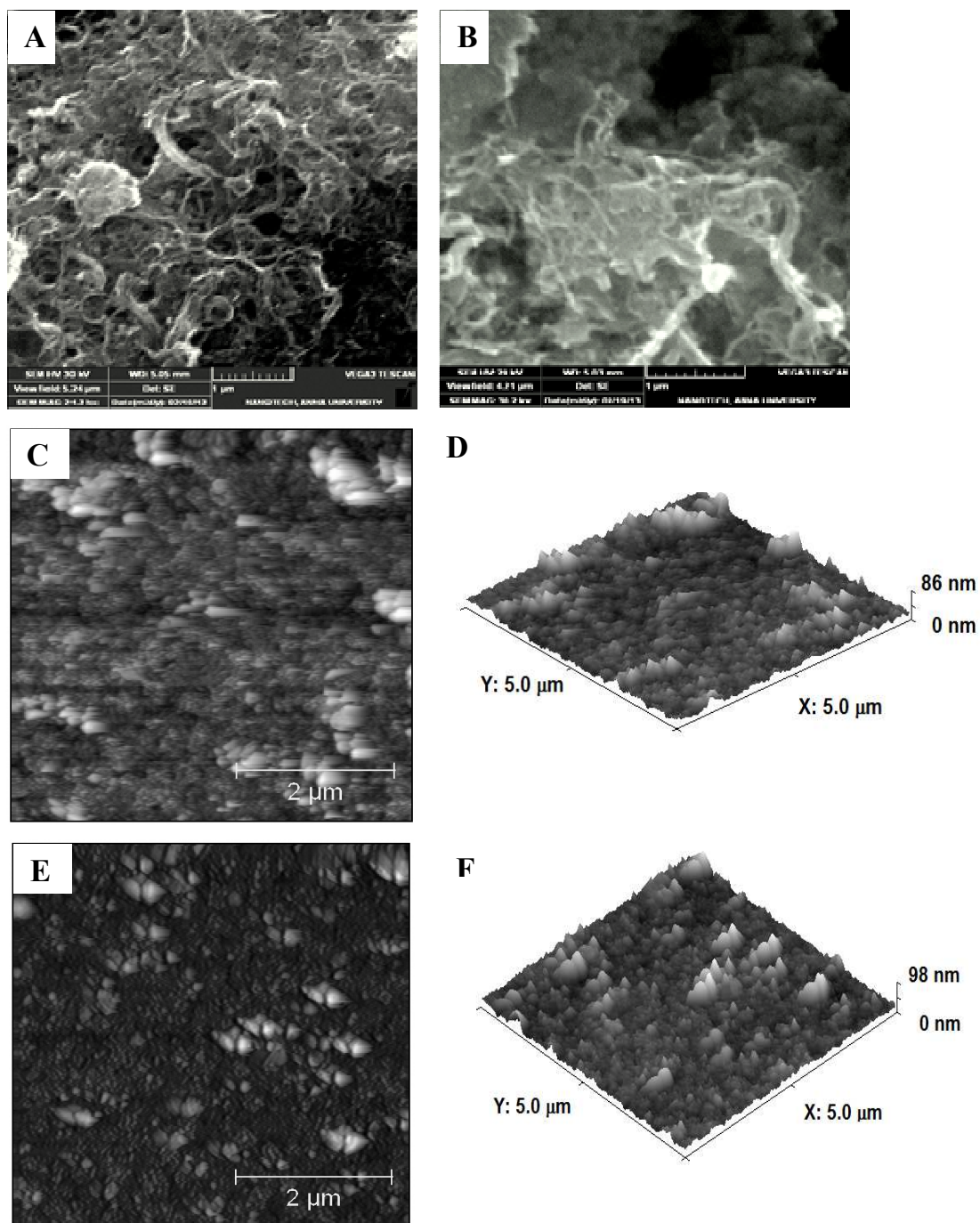


Figure 1

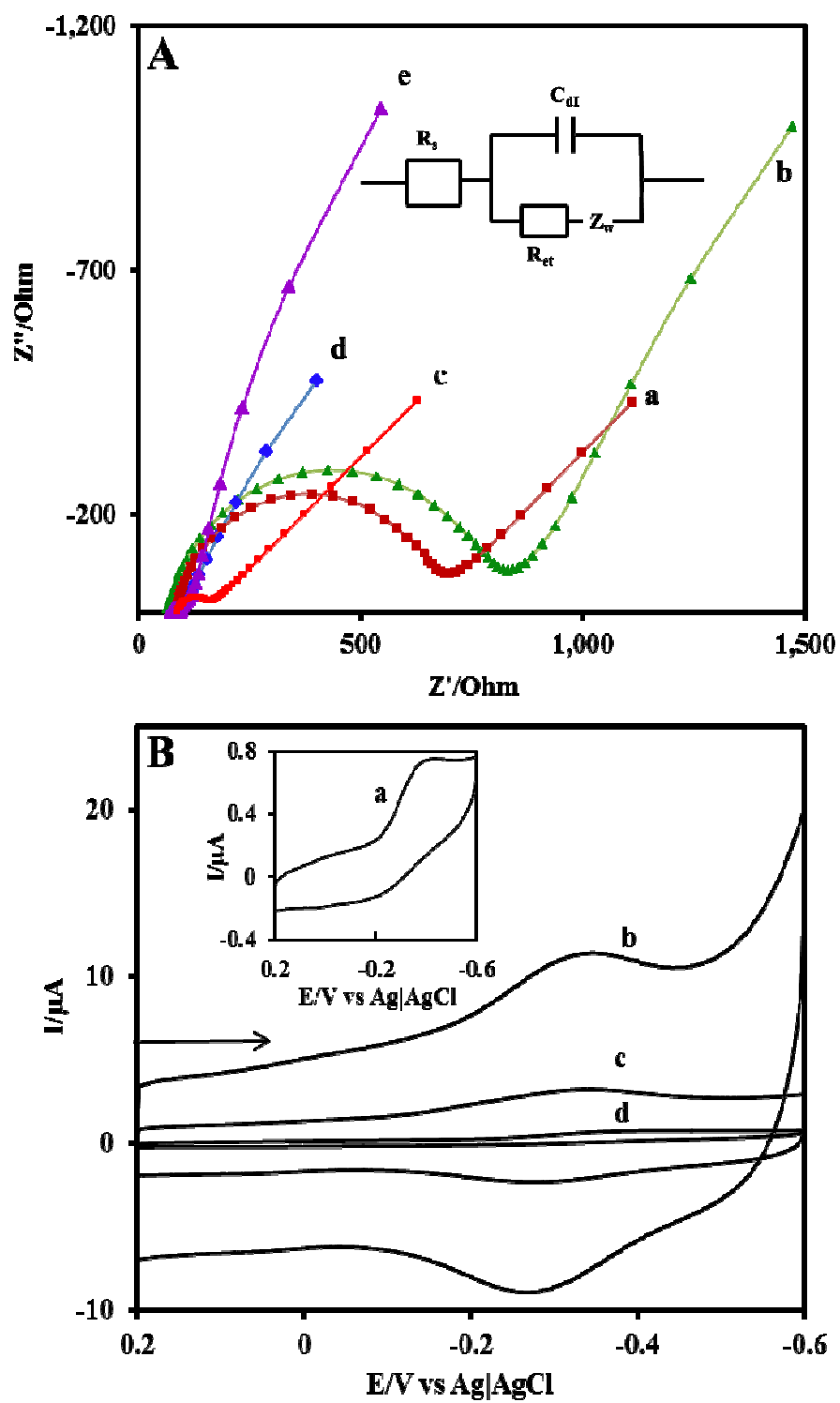


Figure 2

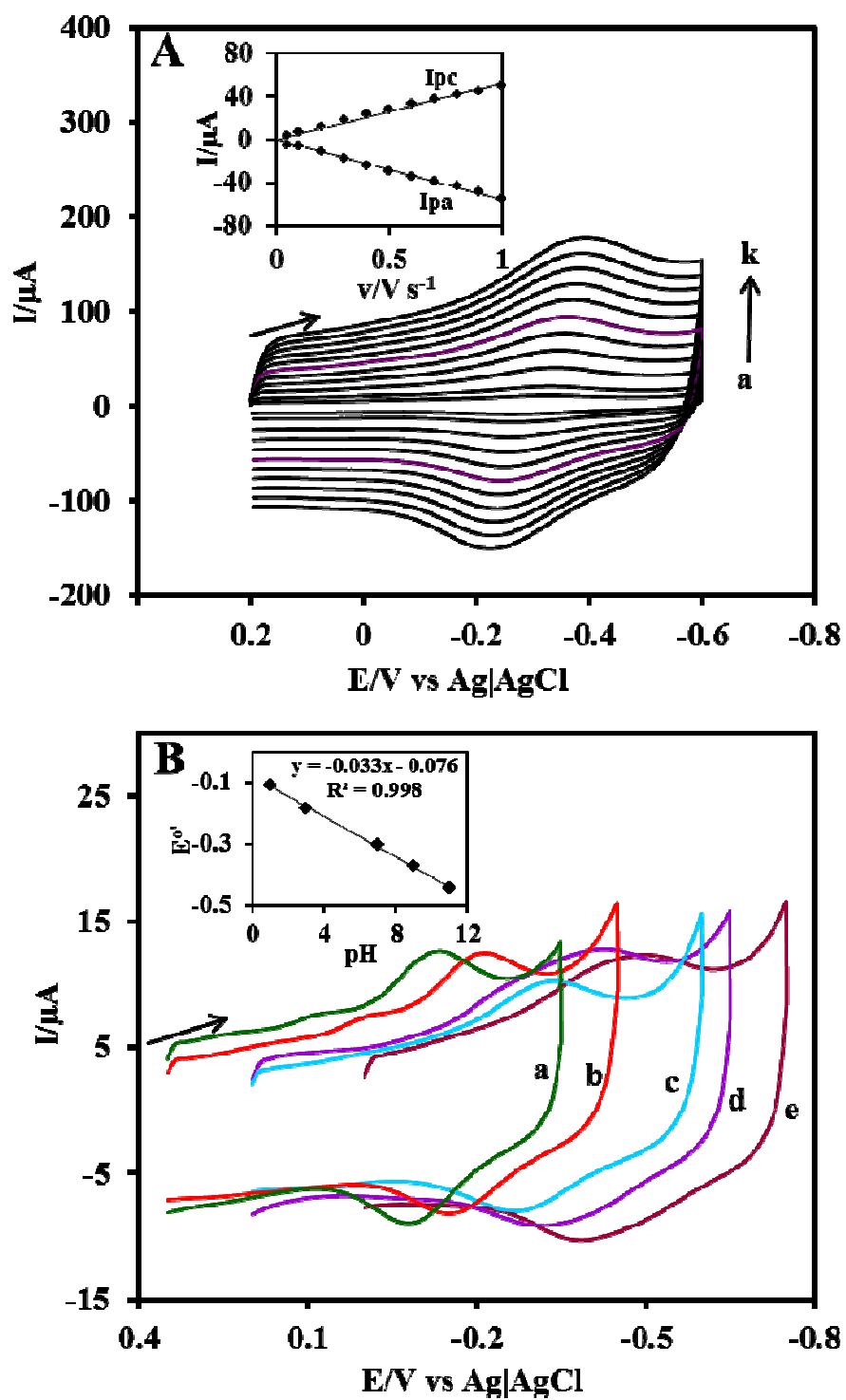


Figure 3

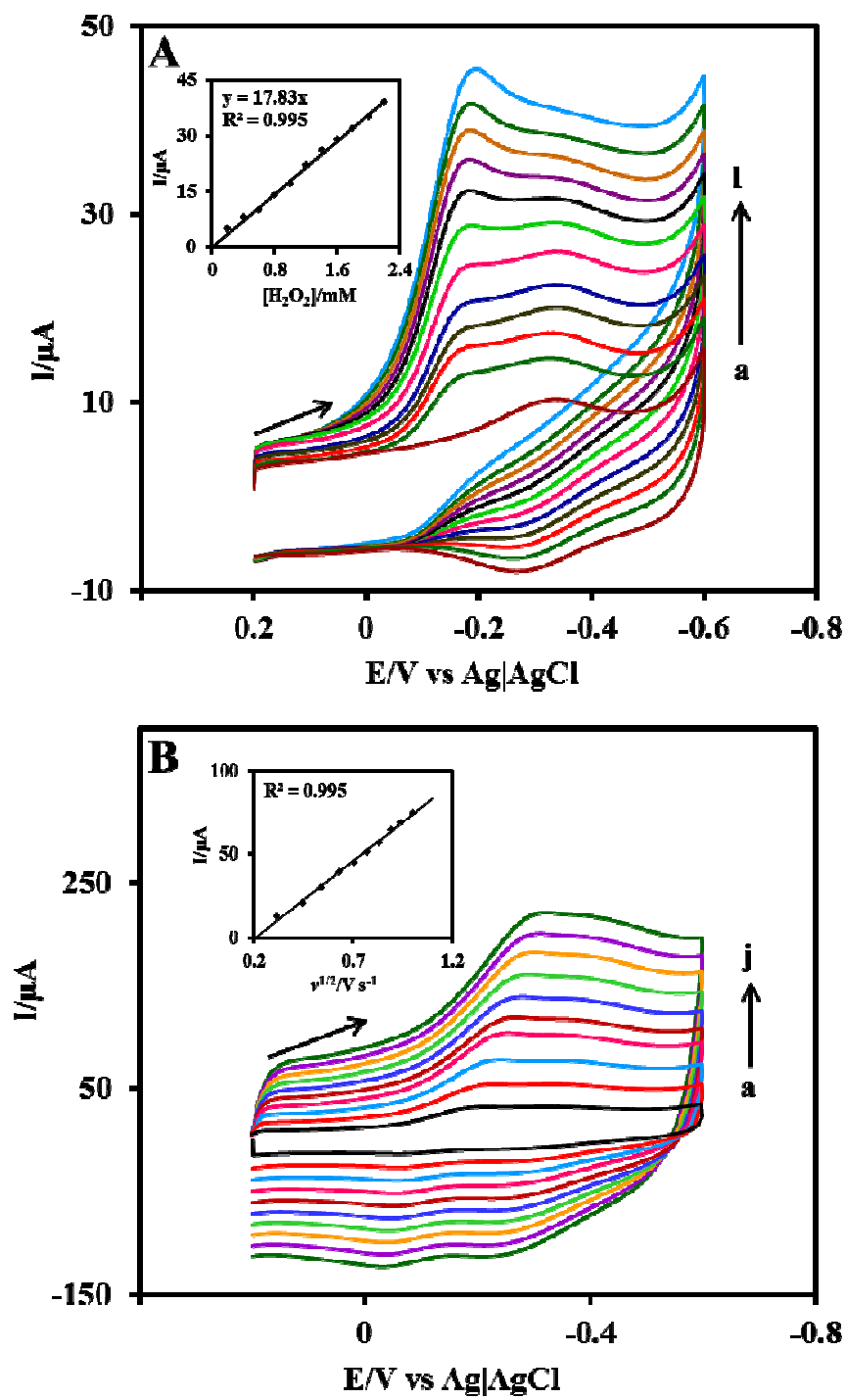


Figure 4

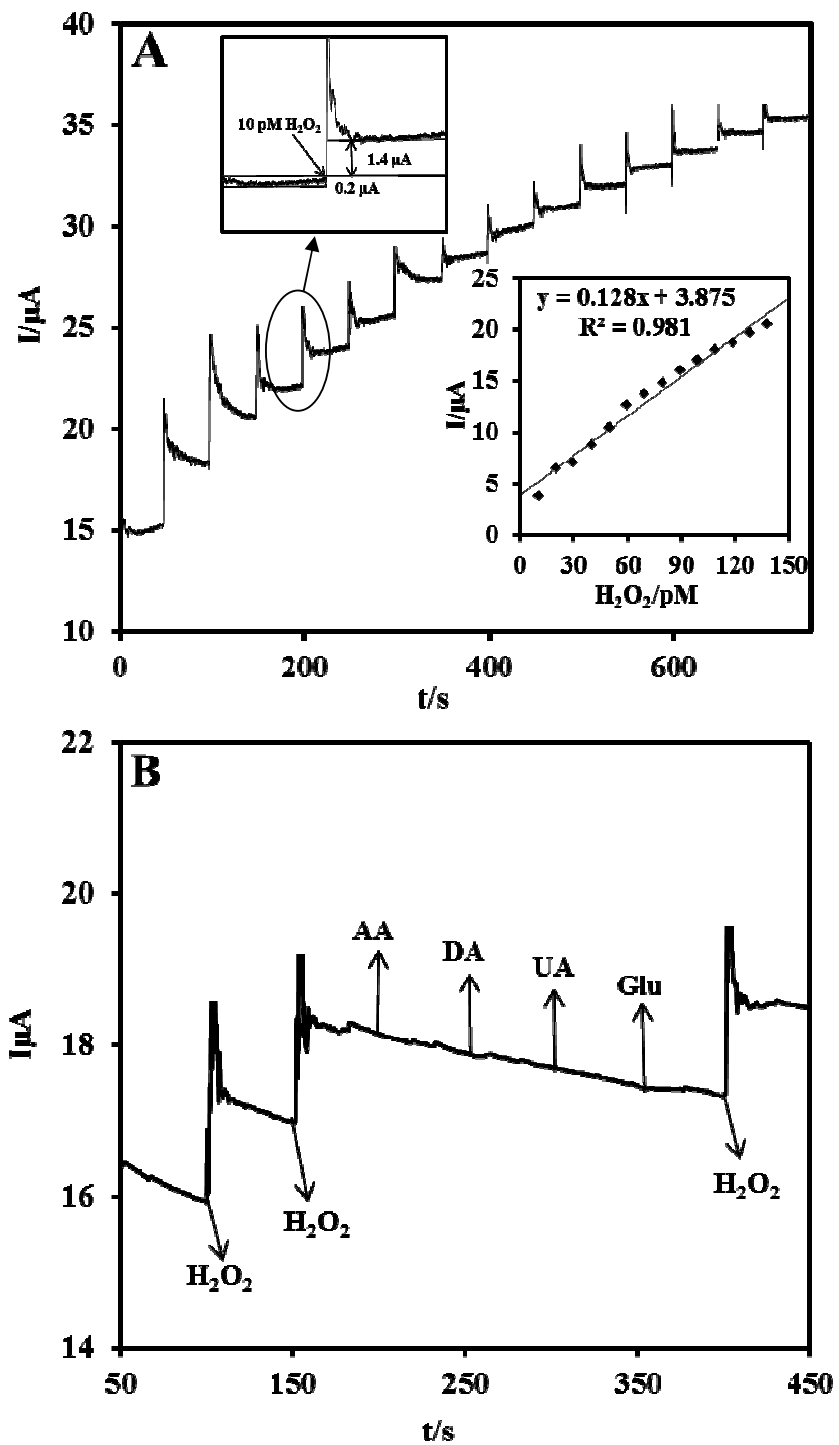


Figure 5